文章编号：1001-9014(2020)04-0513-10

DOI:10.11972/j.issn.1001-9014.2020.04.016

Dim small targets detection based on horizontal-vertical multi-scale grayscale difference weighted bilateral filtering

ZHU Han-Lu[1,2], ZHANG Xu-Zhong[3], CHEN Xin[1], HU Ting-Liang[1], RAO Peng[1*]

(1. Key Laboratory of Intelligent Infrared Perception, Chinese Academy of Sciences, Shanghai Institute of Technical Physics, Chinese Academy of Sciences, Shanghai 200083, China;
2. University of Chinese Academy of Sciences, Beijing 100049, China;
3. Huzhou Center for Applied Technology Research and Industrialization, Chinese Academy of Sciences, Huzhou 313000, China)

Abstract: In order to effectively detect weak and small infrared targets under complex background, a single-frame method based on horizontal-vertical multi-scale grayscale difference (HV-MSGD) is proposed to enhance weak targets, and the strong edges of background are suppressed by the difference between the distance and grayscale values. There is discontinuity between the target area and the surrounding area. To strengthen their differences, HV-MSGD combined with bilateral filtering (BF) can increase the intensity of the target while suppressing the background. Candidate targets are further extracted by adaptive local threshold segmentation and global threshold segmentation. In order to further verify the impact on single-frame detection, the above-mentioned single-frame detection algorithm is combined with an improved untraced Kalman particle filter (UPF) to implement trajectory detection. The experimental results show that this method is better than other methods under weak signal-to-noise ratio (SNR). It can enhance the target while suppressing the background, and the enhancement effect is 6-30 times that of other methods. In the experiments, the input signal-to-noise ratios were 2.78, 1.77, 1.79, 1.13, and 1.16, respectively. After image processing, the background suppression factors (BSFs) are 13.48, 21.33, 11.73, 20.63, and 121.92, and the signal-to-noise ratio gains (GSNRs) are 40.09, 71.37, 27.53, 12.65, and 131, respectively. The probability of detection (Pd) of this method is also superior to other algorithms. When the false alarm rates (FARs) are 5×10^{-4}, 1×10^{-3}, 1×10^{-3}, 1×10^{-5}, and 7×10^{-6}, the Pd values of the five sets using real sequence images are calculated to be 94.4%, 92.2%, 91.3%, 95.6% and 96.7% respectively.

Key words: dim target detection, multi-scale grayscale difference, distance and pixel difference, local threshold segmentation, global threshold segmentation

PACS:07.57.Ty

基于横纵多尺度灰度差异加权双边滤波的弱小目标检测

朱含露[1,2], 张旭中[3], 陈 忻[1], 胡亭亮[1], 饶 鹏[1*]

(1. 中国科学院上海技术物理研究所 中国科学院智能红外感知重点实验室,上海 200083;
2. 中国科学院大学,北京 100049;
3. 中国科学院湖州应用技术研究与产业化中心,浙江 湖州 313000)

摘要:为了有效地检测复杂背景下的红外弱小目标,提出了一种基于横纵多尺度灰度差(HV-MSGD)的方法来增强弱目标,并通过距离和像素差异来实现对背景强边的抑制。目标区域与周围区域之间存在不连续性,为了加强它们的差异,HV-MSGD与双边滤波(BF)相结合,可以在抑制背景的同时提高目标强度。进一步通过自适应局部阈值分割和全局阈值分割来提取候选目标。为了进一步验证对单帧检测的影响,将上述单帧检测算法与改进的无迹卡尔曼粒子滤波器(UPF)相结合,实现轨迹检测。实验结果表明,该方法在弱信噪比

Received date: 2019-08-22, **revised date**: 2019-10-24 **收稿日期**:2019-08-22,**修回日期**:2019-10-24

Foundation items:Supported by the Optical Technology and Instruments Foundation of China (Y7K03213N1)

Biography:ZHU Han-Lu(1992-),Zhejiang, Ph. D. candidate. Research area involves photoelectronic detection and image processing.

*Corresponding author:E-mail: peng_rao@sitp.mail.com.cn

(SNR)下优于其他方法,在抑制背景的同时可以增强目标,增强效果是其他方法的6-30倍。在实验中,输入信噪比分别为2.78,1.77,1.79,1.13和1.16。图像处理后,背景抑制因子(BSFs)分别为13.48,21.33,11.73,20.63和121.92,信噪比增益(GSNRs)分别为40.09,71.37,27.53,12.65和131。该方法的检测概率(Pd)也优于其他算法。当误报率(FARs)为5×10^{-4}, 1×10^{-3}, 1×10^{-3}, 1×10^{-5}和7×10^{-6},计算五组真实序列图像的Pd为94.4%,92.2%,91.3%,95.6%和96.7%。

关 键 词:弱目标检测;多尺度灰度差;距离和像素差;局部阈值分割;全局阈值分割

中图分类号:TN219 **文献标识码**:A

Introduction

Prior knowledge of the shape, size, and texture of dim small target is almost non-existent which limits the development of infrared searching and tracking systems [1-5]. In general, the background is correlated in both the spatial and temporal domains and primarily occupies low-frequency components in the infrared image, whereas the target is less correlated with background and noise, and mainly occupies high frequency components in the image. When such a target is detected under the space-based platform, the background is generally complex with the small target typically appearing against a background of clouds or water, causing the target to become submerged in clutter and background. In situations such as these, it is difficult to separate the target from the complex background, and the filtering process includes a large amount of edge information. This led to the proposal of algorithms capable of protecting the edges while suppressing the background [6-8], such as anisotropy (PM) [9-11] and bilateral filter (BF); [12-14] however, these algorithms do not have the ability to separate the background gradient and target gradient. Dim small targets are discontinuous with their neighboring regions in the image and are concentrated in relatively small areas, which can be considered as uniform and dense regions. The discontinuity is essentially based on the average grayscale difference between adjacent pixels. [15] Researchers proposed local measurement methods to establish different regions and surrounding regions in the image, such as the local entropy operator [15-21] and local mutation weighted entropy, [22-23] which can effectively measure the target area and surrounding area. However, the difference between the measured object and the background grayscale information did not allow the separability of the background gradient and target gradient to be improved.

Based on the above analysis, this study involved the design of a horizontal-vertical multi-scale grayscale difference (HV-MSGD) weighted bilateral filtering (BF) method to detect dim small targets using infrared imaging. The method has the following advantages: (1) the method measures the discontinuity between the target area and background area by comparing the regional standard deviation to determine the size of the window; (2) the HV-MSGD weighted operator is used to realize the expansion of the difference between the target and background area by using the size of the window to achieve target enhancement; (3) background edge information is suppressed in consideration of the difference between the distance and grayscale value of each pixel in the image; (4) the combination of global and local threshold segmentation (GLTS) prevents extremely strong signals such as those of noise and clutter to influence the target itself, which eliminates noise elements and detects the real target signal. In other words, HV-MSGD is combined with BF to improve the separability of the target and background gradient, thereby increasing the energy of the target while suppressing the edge information in the image. Experiments show that this method is superior to other algorithms in terms of its ability to detect weak targets.

1 Single frame detection of dim targets

1.1 Target signal enhancement—HV-MSGD

In an infrared image, the grayscale of the target pixels differs greatly from that of the surrounding pixels with a large discontinuity in the luminance. This discontinuity fundamentally determines that the nature of the average grayscale can be obtained from the pixels adjacent to the target. [24] This led researchers to use multi-scale grayscale methods to quantitatively analyze images to distinguish the difference between the target and the surrounding area. [25-27] These methods mainly rely on image entropy to obtain multi-scale grayscale difference, the amount of calculation is huge, and the effect on weak targets is not obvious. These attempts encouraged us to develop an improved multi-scale grayscale difference method to enhance the weak signals and to overcome situations in which the thermal intensity measurements of the target are similar to the those of the background.

Small and weak targets are concentrated in a small, uniform and compact area, which has discontinuity with the surroundings. Therefore, this paper designs a method to calculate this discontinuity and achieve enhancement of weak targets. The standard deviation of the image reflects the clutter fluctuations of the images, so the appropriate window size can be selected to obtain the MSGD of the image by comparing the LG-SGD.

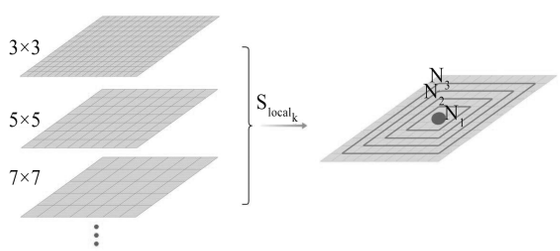

Fig. 1 Standard deviation calculation module for k windows
图1 窗口k的标准差计算模块

The image is traversed from top to bottom and left to right, and the area is divided into k neighborhoods surrounding the pixels. As shown in Fig. 1, taking k = 3 as an example, N_1, $N_2$and N_3 are three differential regions surrounding the central pixel, and the sizes of their windows are 3×3, 5×5, and 7×7, respectively. The grayscale average of the kth region is expressed as:

$$v_{N_k}=\frac{1}{n_{N_k}}\sum_{(m,n)\in N_k} I(m,n) \quad , \quad (1)$$

where k is the number of differential regions with values k =1,2,3, . . . , k, the set N_k represents the differential region, n_{N_k} represents the number of pixels in region N_k, and $I(m,n)$ represents the grayscale of pixels in the region N_k. In actual operation, the sizes of windows 3, 5, 7, 9, and 11 are primarily used for calculations and selections. Then the local standard deviation S_{local_k} in the kth region is as follows:

$$S_{local_k}=\frac{1}{n_{N_k}}\sqrt{\sum_{(m,n)\in N_k}(I(m,n)-v_{N_k})^2} \quad . \quad (2)$$

According to Eq. 2, for a heterogeneous region, the local grayscale standard deviation is large when the window is small, whereas the local grayscale standard deviation is small for a homogeneous region in the same window. Figure 2 shows the response of different boundaries at different scales, with the peak response of the horizontal or vertical boundary appearing in a large window. In contrast, a strong peak response occurs at the point target in a small window, indicating that a small-scale window affects the intensity of the point target, but has no effect on the boundary. Thus, selection of a window of the appropriate size can enhance the signal of the target. The size of the window can be determined by comparing the standard deviation within a region:

$$W_{size}=\underset{W_{size}}{\operatorname{argmin}}(S_{local_1},S_{local_2},\cdots,S_{local_k}) \quad . \quad (3)$$

The determined window size W_{size} is used to obtain the grayscale value of the predicted point by using the HV-MSGD, and enhancement of the target area is achieved by the difference in response between the horizontal and vertical boundaries. The specific implementation is shown in Fig. 3. First, the gradient difference of the vertical grayscale is calculated by Eqs. 1-2, after which these two equations are used to calculate the gradient difference of the horizontal grayscale before the results with the enhanced target is obtained. The specific calculation process is as follows:

$$\begin{bmatrix} f_{11} & \cdots & f_{n1} \\ \vdots & \ddots & \vdots \\ f_{1n} & \cdots & f_{nn} \end{bmatrix} \overset{VGD}{\Rightarrow} \left[\sum_{i=1}^{n}(f_{1i}-\frac{1}{n}\sum_{i=1}^{n}f_{1i})^2 \quad ,\cdots, \quad \sum_{i=1}^{n}(f_{ni}-\frac{1}{n}\sum_{i=1}^{n}f_{ni})^2 \right]$$

$$=\left[VGD_{11} \quad ,\cdots, \quad VGD_{1n} \right] \overset{HGD}{\Rightarrow} \sum_{i=1}^{n}(VGD_{1i}-\frac{1}{n}\sum_{i=1}^{n}VGD_{1i})^2 =$$

$$=HVGD(x,y) \quad , \quad (4)$$

where $f_{11}\cdots f_{nn}$ is the corresponding value of the n × n region, the horizontal grayscale value $[\,VGD_{11} \quad \cdots \quad VGD_{1n}\,]$ is obtained after the vertical gradient difference is calculated, then the final target enhancement value $HVGD(x,y)$ is obtained by calculating the horizontal grayscale gradient difference. In summary, the specific processing of this algorithm is shown in the following module:

Algorithm: HV-MSGD

Input: original image F

Output: window size, grayscale value processed by HV-MSGD

for every pixel in F **do**

Set different window sizes, mainly 3, 5, 7, 9, 11

Calculate the average of the different regions by formula 1

Calculate the local standard deviation of the different regions by formula 2

Get the size of the window W_{size} by formula 3

Calculate HV-MSGD in $W_{size}\times W_{size}$ area as formula 4, which is processed predicted value

end for

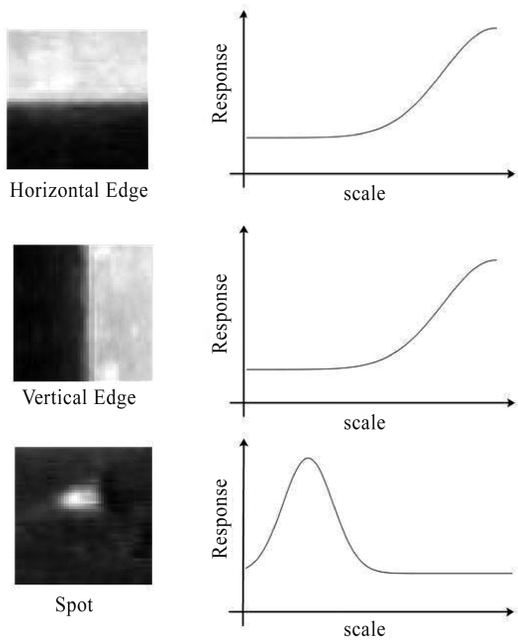

Fig. 2 The response of different boundaries at different scales
图2 不同尺寸下不同边界的响应

1.2 Background estimation—BF

Bilateral filtering can smooth the image while estimating the background of the image. The filter employs two weights: the filter coefficient $c(x,y)$ determined by the geometric spatial distance and the filter coefficient $s(x,y)$ determined by the difference in grayscale similarity. In the sampling procedure, which considers the relationship between pixels by using the spatial distance and grayscale similarity difference, the two coefficients are expressed as follows:

$$c(x,y)=e^{-\frac{(x^2+y^2)}{2\sigma_d^2}} \quad , \quad (5)$$

$$s(x,y)=e^{-\frac{(f(\xi,\eta)-f(x,y))^2}{2\sigma_s^2}} \quad . \quad (6)$$

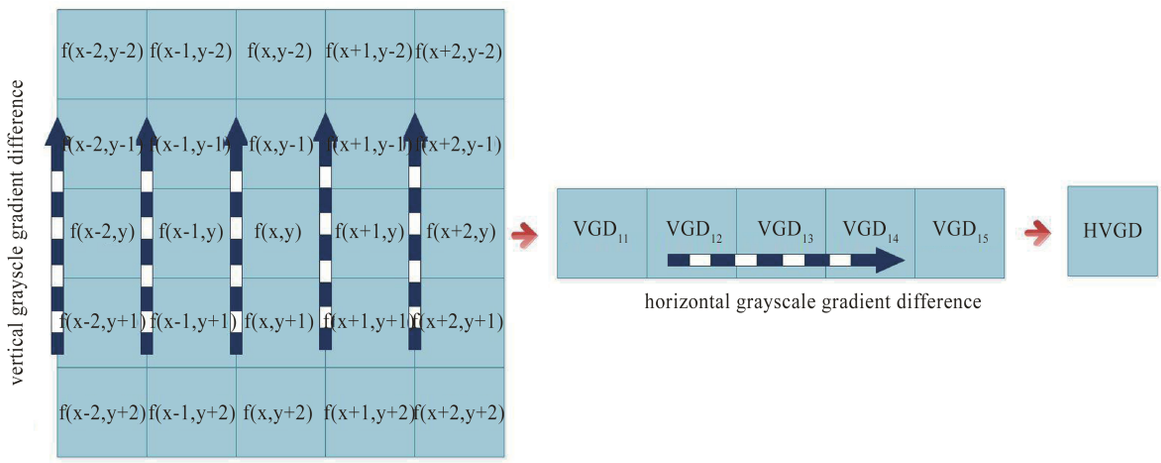

Fig. 3 calculate the HV-MSGD weighting operator
图3 横纵多尺度灰度差异算子计算

The weight coefficient is composed of the two:

$$w_{ds}(x,y) = c(x,y)\cdot s(x,y) \quad , \quad (7)$$

where σ_d and σ_s are the bandwidth coefficients of the two filter coefficients, $f(\xi,\eta)$ is grayscale gray of the N × N region of $f(x,y)$, then the background estimation $h(x,y)$ can be obtained:

$$h(x,y) = \Big(\sum_{N\times N} w_{ds}(x,y)\Big)^{-1}\cdot \sum_{N\times N} f(x,y)\cdot w_{ds}(x,y). \quad (8)$$

Subtracting the result of the background estimation from the original image, the background suppression image out(x,y) is obtained as follows:

$$\mathrm{out}(x,y) = f(x,y) - h(x,y) \quad , \quad (9)$$

where the out(x,y) is the final background suppression image. It is worth noting that the image needs to be normalized during the calculation process. Then the candidate target is extracted by GLTS.

1.3 Threshold segmentation

The target and its background are discontinuous[15-16]. The image $\mathrm{Img_{pro}}$ is processed by HV-MSGD weighted BF, which enlarges the discontinuity between the target region and the background region. This method successfully enhances the target, and restrains the background clutter and noise effectively. The overall process to detect a dim small target is illustrated in Fig. 4.

The threshold segmentation process adopts a method that combines global and local threshold segmentation to determine dim small targets. The global threshold segmentation is an adaptive threshold segmentation T_G for the entire image and is obtained as follows:

$$T_G = t\times\sigma + m \quad , \quad (10)$$

$$\mathrm{Seg_G} = \begin{cases} 1 & \mathrm{Img_{pro}}(i,j) > T_G \\ 0 & \mathrm{Img_{pro}}(i,j) \leqslant T_G \end{cases} \quad , \quad (11)$$

where σ is the standard deviation of the image, m is the average of the image, and t is an odd number greater than 3. Then we can get the image Seg_G of global threshold segmentation by Eq. 11. $\mathrm{Img_{pro}}(i,j)$ is the grayscale value of the image processed by HV-MSGD weighted BF at point (i,j). Local threshold segmentation divides the image into $N\times N$ regions and calculates the ith segmentation threshold value T_{Li} for different regions respectively, using Eq. 12:

$$T_{Li} = t\times\sigma_i + m_i \quad , \quad (12)$$

$$\mathrm{Seg_L} = \begin{cases} 1 & \mathrm{Img_{pro}}(i,j) > T_{Li} \\ 0 & \mathrm{Img_{pro}}(i,j) \leqslant T_{Li} \end{cases} \quad , \quad (13)$$

where σ_i is the standard deviation of the ith partition region, $i=1,2,3,\cdots,N\times N$, and m_i is the average of the ith partition region. Then we can get the image Seg_L of local threshold segmentation by Eq. 13. The algorithm is designed to detect an entire single-frame containing a small target is described in the following module. The two equations use the same threshold t.

$$\mathrm{Seg} = \mathrm{Seg_G}\cdot\mathrm{Seg_L} \quad . \quad (14)$$

Algorithm: threshold segmentation

Input: image P processed by HV-MSGD and BF

Output: image processed by threshold segmentation

Calculate the global threshold according to Eq. 10

for every pixel in p **do**

Divide the image into $N\times N$ regions

Calculate the local threshold T_{Li} for every region according to Eq. 12

end for

Segment the image according to global and local thresholds by Eq. 14 to obtain the final image H

2 Trajectory detection

On the basis of the procedure for single-frame detection described in Sec. 2, further verification of the effect of the proposed method, combined with the improved UPF, is conducted by predicting the target position by the probability data association (PDA) and to finally obtain the motion trajectory. According to the actual moving speed of the target, the frame rate and other factors, setting the range of the suspected position to 10 pixels,

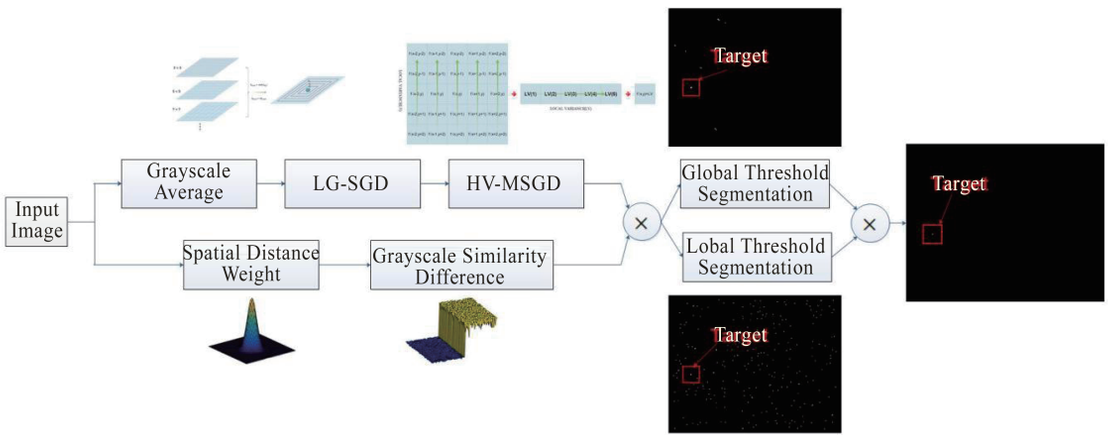

Fig. 4 The detection process of the entire dim small target
图4 整个小目标探测流程示意图

to solve the tracking accuracy. For the improved UPF, we detect the single-frame according to Sect. 1, to obtain the positions of suspected target points, and then estimate the suspected target points probabilistically to obtain the predictive value, and according to literature [28] we can get the final target position. For the PDA, we can get the associated probability $\beta_i(k)$ by following:

$$\beta_i(k)=\frac{e_i(k)}{b(k)+\sum_{j=1}^{m_k}e_j(k)}\left(i=1,2,\cdots,m_k\right), \quad (15)$$

$$e_i(k)=\exp\{-\frac{1}{2}\left[Z(k)-\hat{Z}(k|k-1)\right]^T X^{-1}(k)\left[Z(k)-Z(k|k-1)\right]\}, \quad (16)$$

$$b(k)=\lambda(2\pi)^{\frac{m}{2}}|X(k)|^{\frac{1}{2}}(1-P_dP_G)/P_d \quad . \quad (17)$$

where $Z(k)=\left\{Z_1(k),Z_2(k),\cdots,Z_{m_k}(k),\right\}$ represents all valid measurement sets that fall within the target tracking gate at time k, m_k represents the number of effective measurement at time k, $X(k)$ is covariance matrix, P_d is the detection probability with a value of 1, P_G is the threshold probability with a value of 0.97. The steps of the process are shown in Fig. 5 and the specific algorithm is described in Algorithm 3:

Algorithm: Trajectory detection

Input: image sequence processed by single frame detection as Sect. 1

Output: motion trajectory

Setting parameters: process noise N_p, measurement noise N_m, covariance matrix X, target initial state

for each image in the sequence do

Detect the single-frame according to Sect. 1, to obtain the positions of suspected target points

Estimate the suspected target points probabilistically using PDA to obtain the predictive value

Calculate the final target position using UPF based on the predictive value

end for

Plot the target positions of the image sequence to obtain the trajectory

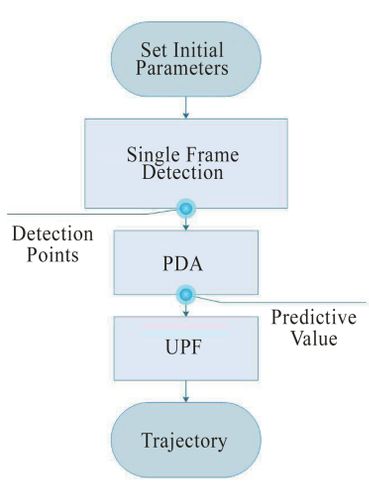

Fig. 5 Flow chart of trajectory detection
图5 轨迹探测示意图

3 Analysis of experimental results

3.1 Experimental environment and images

The effectiveness of the infrared dim small target detection algorithm based on HV-MSGD weighted BF was verified by using five sets of real infrared image sequences for experimental comparison. The operating environment of this experiment is MATLAB2014b on a Windows 10 (64-bit) system with 2.5 GHz CPU, an Intel Core i5 processor, and 8 GB memory. The parameters used in the experiment were σ_d=0.8, σ_s=0.3, t = 3. The choice of these three parameters needs to be determined according to the images in different scenes. σ_d controls the spatial distance, when the value is large, the effective spatial range is larger, and the edge points can also obtain larger weights, and the denoising effect is obvious. σ_s controls the grayscale change in the image. The larger grayscale difference, the higher the weight value can be obtained, but the small edge will be affected, and there is no good edge-preserving effect. t mainly affects the result of threshold segmentation.

When t is too small, the false alarm rate will increase. When the value is too large, the true target may be removed, resulting in a missed alarm. Therefore, it is necessary to select according to actual conditions. In this manuscript, these three values are obtained by experiment based on the specific image. Figure 6 shows the results of processing five random images by our method, where (a) is the input image, (b) is the 3D view of the input image, (c) is the image processed by HV-MSGD weighted BF, (d) is the 3D image processed by HV-MSGD weighted BF, (e) is the processed threshold segmentation image, and (f) is the 3D threshold segmentation image. The results in Fig. 6 show that the background is obviously suppressed by our method, and the target is strongly enhanced. Even against a background with strong edges, the target is well detected and the threshold segmentation is excellent. In addition, in the experiment, we compared the ability of BF, [9] TDLMS, PM, [12] LCM, [24] NWIE, [26] and our method to detect the target. The resultant images shown in Fig. 7, which shows that the background signal remains strong after processing by the other algorithms, but is significantly suppressed by our method.

3.2 Evaluation method

The performance of these methods was compared by using three indicators, i. e., the gain of the signal-to-noise ratio (GSNR), background suppression factor (BSF), and receiver operating characteristic (ROC) curve for the quantitative evaluation of the background suppression and target detection performance. The indicators are defined as follows:

$$\mathrm{GSNR} = \frac{\mathrm{SNR}_{\mathrm{out}}}{\mathrm{SNR}_{\mathrm{in}}}, \quad (18)$$

$$\mathrm{BSF} = \frac{\sigma_{\mathrm{in}}}{\sigma_{\mathrm{out}}}, \quad (19)$$

$$\mathrm{SNR} = \frac{|\mu_{\mathrm{target}} - \mu_{\mathrm{background}}|}{\sigma_{\mathrm{noise}}}, \quad (20)$$

where $\mathrm{SNR}_{\mathrm{out}}$ and $\mathrm{SNR}_{\mathrm{in}}$ are the local SNR of the target before and after background suppression, σ_{in} and σ_{out} are the standard deviations of the local background area of

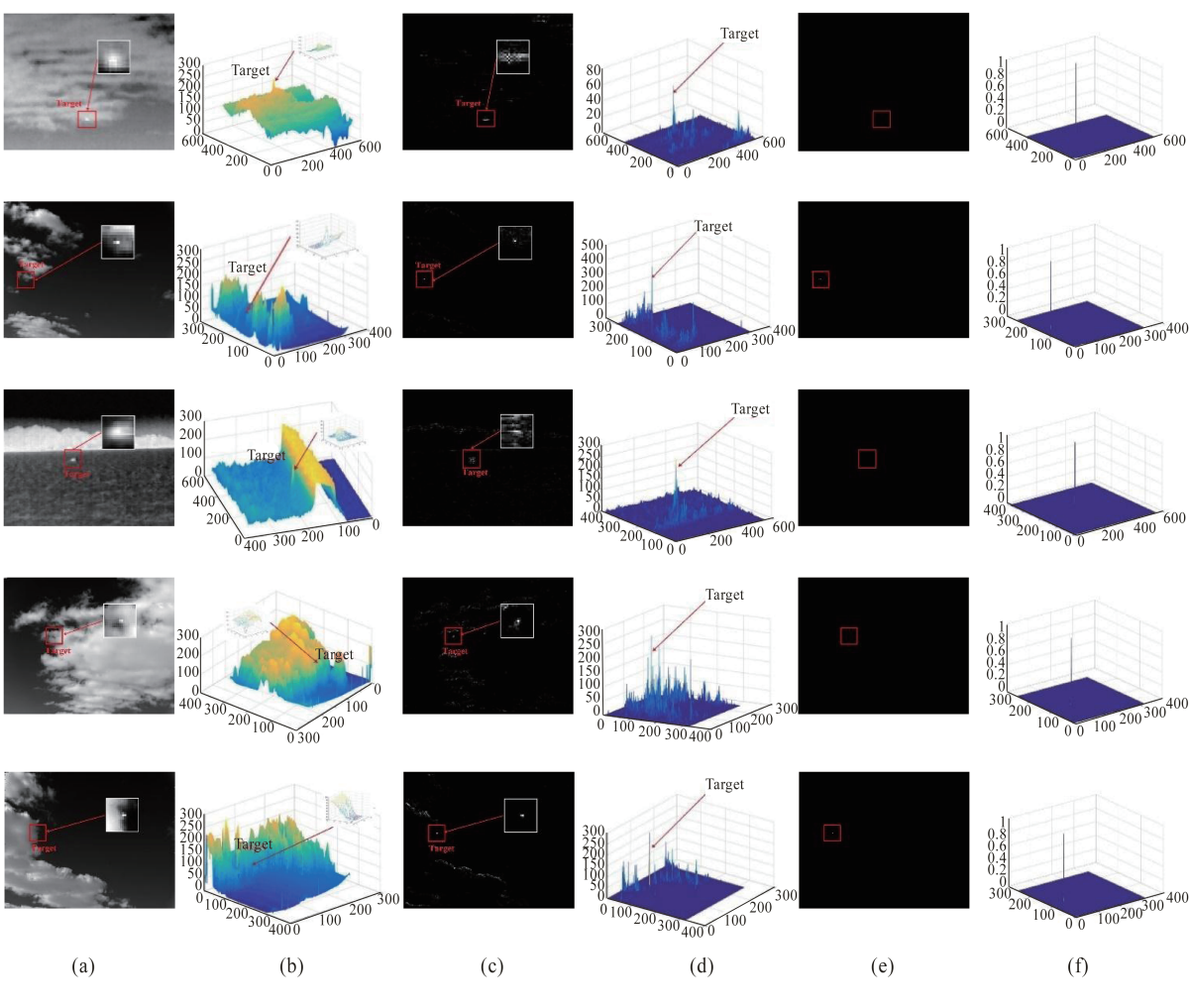

Fig. 6 the results of five images that processed by our method, (a) is the input image, (b) is the 3D view of the input image, (c) is the image processed by HV-MSGD, (d) is a 3D image processed by HV-MSGD, (e) is a threshold segmentation image processed by (c), (f) is a 3D threshold segmentation image processed by (c)

图6 经过本文提出方法处理后的5幅图像结果 (a)是输入图像,(b)是输入图像的三维视图,(c)是经过HV-MSGD处理后的图像,(d)是经过HV-MSGD处理后的三维图像,(e)阈值分割图像,(f)阈值分割三维图像

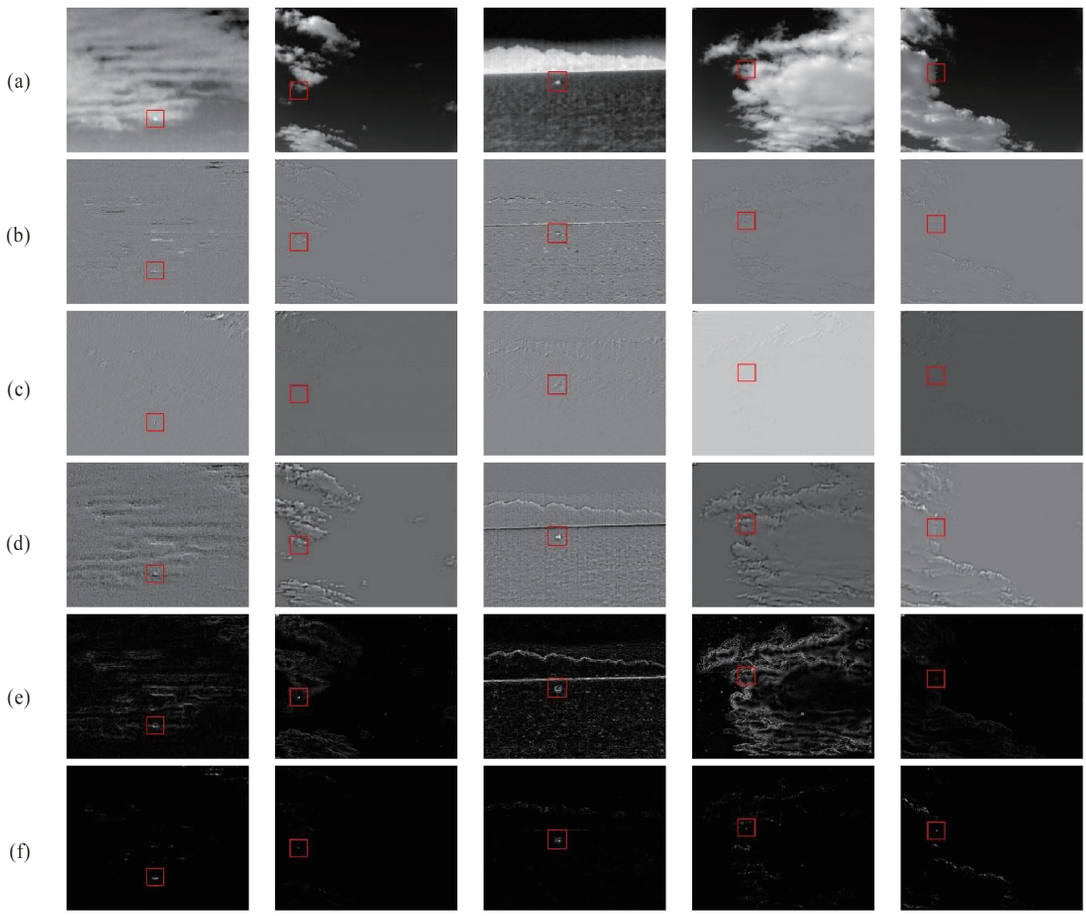

Fig.7 Background suppression results of different algorithms in different scenarios (a) original image, (b) BF filtering result, (c) TDLMS filtering result in literature 15, (d) PM filtering result, (e) LCM filtering result of in literature 24, (f) NWIE, (g) filtering result of our method

图7 在不同场景下不同算法HV-MSGD结果(a)原始输入图像,(b)BF结果,(c)TDLMS结果,(d)PM结果,(e)LCM结果,(f) NWIE结果,(g) HV-MSGD的结果

the target before and after background suppression, $\mu_{\text{target}}$and $\mu_{\text{background}}$ are grayscale peak value of the target and background areas, and σ_{noise} is the standard deviation of the local background area.

The evaluation index (Eqs. 18-19) was used to compute BSF and GSNR of the image shown in Fig. 7, and the results are listed in Table 1. The BSF and GSNR results of the images processed by our method are superior to those obtained by other methods. The SNR values used as input were 2.78, 1.77, 1.79, 1.13 and 1.16, respectively. After image processing, the BSF values were 13.48, 21.33, 11.73, 20.63, and 121.92, and the GSNR values were 40.09, 71.37, 27.53, 12.65, and 131, respectively.

The ROC curve describes the mutual constraint relationship between the probability of detection (Pd) and the false alarm rate (FAR). The value of Pd for different values of FAR can be obtained by changing the detection threshold t in Eqs. 10 and 12, where P_d and P_f are the values of Pd and FAR, calculated as follows:

$$P_d = \frac{N_{\text{target}}}{T_{\text{target}}} \quad , \quad (21)$$

$$P_f = \frac{N_{\text{pixel}}}{T_{\text{pixel}}} \quad , (22)$$

where N_{target} is the number of detected targets, T_{target} is the number of actual targets, N_{pixel} is the number of pixels of the false target, and T_{pixel} is the number of all pixel points in the detection images.

Based on the description of ROC, the ROC values of the five sequences are plotted in Fig. 8, which clearly shows that the values of Pd obtained using our method are more accurate than those obtained with the other algorithms. Five sets of images that formed real sequences were processed using FARs of 5×10^{-4}, 1×10^{-3}, 1×10^{-3}, 1×10^{-5}, and 7×10^{-6} to obtain Pd values of 94.4%, 92.2%, 91.3%, 95.6%, and 96.7%, respectively. In addition, we compared the average values of BSF and GSNR for these five sequences obtained with the different algorithms, and present the results in Table 2. The five sequences contain 75, 90, 65, 90 and 90 images, respectively. Sequence 1 is on thick cloud background, sequence 2 is on bright cloud background, sequence 3 is on bright edge background, and sequence 4 is on blocky cloud background, and sequence 5 is on

Table 1 BSF and GSNR of different five images processed by different methods
表1 经过不同方法处理后的BSF和GSNR

Image	Input		BF		TDLMS		PM	
	SNR_{in}	σ_{in}	BSF	GSNR	BSF	GSNR	BSF	GSNR
Image 1	2.78	30.05	2.15	6.56	8.19	8.5	1.73	3.26
Image 2	1.77	42.87	4.08	13.12	18.72	7.98	1.33	3.12
Image 3	1.79	59.95	1.82	4.33	6.37	4.57	1.77	4.33
Image 4	1.13	36.73	1.38	8.19	11.77	4.92	0.69	1.5
Image 5	1.16	29.26	7.1	20.89	31.46	14.24	2.56	7.12

Image	LCM		NWIE		Our method	
	BSF	GSNR	BSF	GSNR	BSF	GSNR
Image 1	2.63	7.7	4.55	1.59	13.48	40.99
Image 2	2.63	8.89	4.43	18.94	21.33	71.37
Image 3	1.61	2.98	2.72	16.98	11.73	27.53
Image 4	1.09	1.92	8.46	7.82	20.63	12.65
Image 5	4.41	4.59	21.52	21.32	121.92	131

bright and thick cloud background. In the experiment, the average SNRs were 2.23, 0.56, 1.21, 2.09, and 1.17, respectively. After using our method for image processing, the average BSFs were 5.38, 5.46, 14.71, 23.26, and 7.47, and the GSNRs were 33.97, 15.64, 55.18, 81.8, and 47.51, respectively. The area under curve (AUC) is defined as the area enclosed by the coordinate axis under the ROC curve. Because the AUC can intuitively characterize the superiority or inferiority of each algorithm, we calculated the AUC of five sequences using different algorithms. These results are provided in Table 3. Moreover, we further verified the effectiveness of our method by using the trajectory detection algorithm mentioned in Sect. 2 to compute the trajectory. Figures 9-10 show the trajectory image and bias pixels, which are within two pixels. The conclusion that can be made from Figs. 9-10 are that the proposed method can achieve high probabilities of detection as well as low false alarm rates for different target movements.

4 Conclusions

This study investigated the problem associated with detecting small targets that are weak infrared emitters. Our efforts mainly focused on increasing the discontinuity between the target region and the background region by using HV-MSGD, which improved the separability of the target from the background. In addition, background edge information was suppressed by BF, and the target was finally extracted by the GLTS algorithm. A comparison of the results with those of other methods on five images showed that our method is superior to other methods in both GSNR and BSF, and the enhancement effect is 6~30 times that of the other methods. In addition, comparison of the average $\overline{GSNR}$ and $\overline{BSF}$ of five sequences that

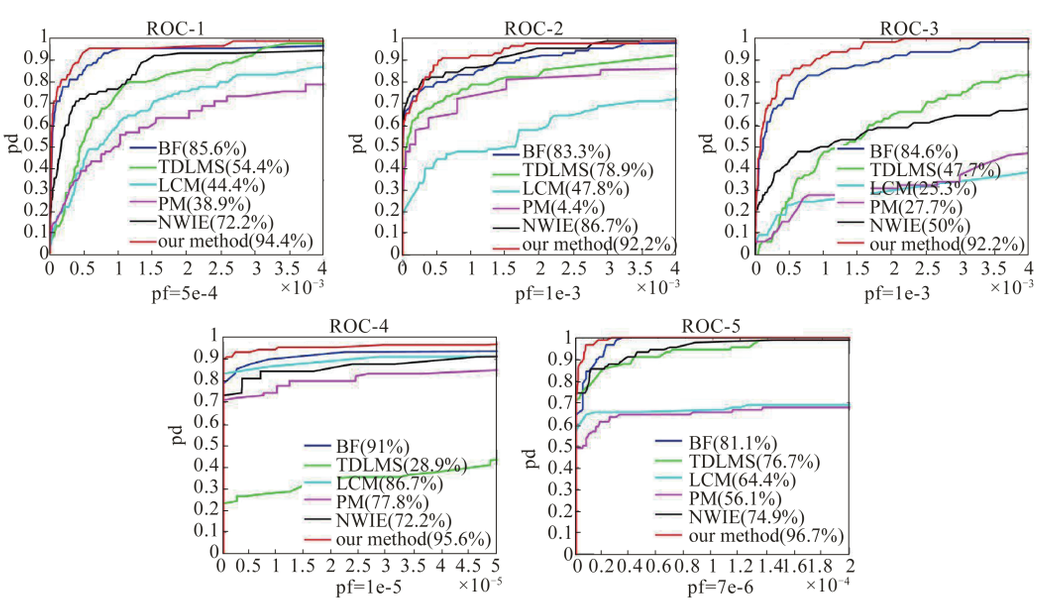

Fig.8 ROC of the five sequences
图8 五个序列的ROC曲线

Table 2 the average of BSF and GSNR for five sequences
表2 五个序列的BSF和GSNR的平均值

IMAGE	Frame number	Input		BF		TDLMS		PM	
		$\overline{\sigma_{in}}$	$\overline{SNR_{in}}$	$\overline{BSF}$	$\overline{GSNR}$	$\overline{BSF}$	$\overline{GSNR}$	$\overline{BSF}$	$\overline{GSNR}$
Seq 1	75	25. 72	2. 23	3. 13	4. 36	1. 01	3. 58	3. 1	2. 31
Seq 2	90	8. 36	0. 56	1. 22	5. 72	2. 42	5. 12	1. 28	4. 56
Seq 3	65	6	1. 21	9. 3	10. 68	2. 55	8. 24	6. 16	7. 37
Seq 4	90	32. 78	2. 09	2. 64	9. 49	5. 71	7. 61	1. 19	4. 01
Seq 5	90	11. 53	1. 17	1. 07	6. 77	1. 2	4. 86	1. 95	3. 89
Average	–	17. 22	1. 44	3. 12	7. 32	2. 64	5. 82	2. 51	4. 33

IMAGE	Frame number	LCM		NWIE		Our method	
		$\overline{BSF}$	$\overline{GSNR}$	$\overline{BSF}$	$\overline{GSNR}$	$\overline{BSF}$	$\overline{GSNR}$
Seq 1	75	3. 1	1. 27	1. 98	6. 04	5. 38	33. 97
Seq 2	90	1. 01	2. 02	2. 40	9. 42	5. 46	15. 64
Seq 3	65	4. 76	3. 13	1. 34	13. 73	14. 71	55. 18
Seq 4	90	1. 17	7. 94	3. 17	10. 25	23. 26	81. 8
Seq 5	90	2. 94	1. 61	1. 74	13. 1	7. 47	47. 51
Average	–	2. 45	3. 27	2. 13	10. 51	11. 26	36. 47

Table 3 AUC of five sequences in different algorithms
表3 五个序列在不同算法下的AUC

P_d	Seq 1 $\overline{SNR_{in}}$ = 2.23	Seq2 $\overline{SNR_{in}}$ = 0.56	Seq 3 $\overline{SNR_{in}}$ = 1.21	Seq 4 $\overline{SNR_{in}}$ = 2.09	Seq 5 $\overline{SNR_{in}}$ = 1.17	Average $\overline{SNR_{in}}$ = 1.44
BF	0. 9200	0. 9470	0. 8704	0. 9253	0. 9525	0. 9230
TDLMS	0. 7202	0. 7427	0. 4342	0. 4765	0. 9334	0. 6614
LCM	0. 6374	0. 8439	0. 2871	0. 9056	0. 6738	0. 6696
PM	0. 5551	0. 7645	0. 3061	0. 8577	0. 6338	0. 6234
NWIE	0. 8477	0. 9167	0. 5578	0. 8614	0. 9507	0. 8269
Our method	0. 9320	0. 9577	0. 9349	0. 9847	0. 9761	0. 9571

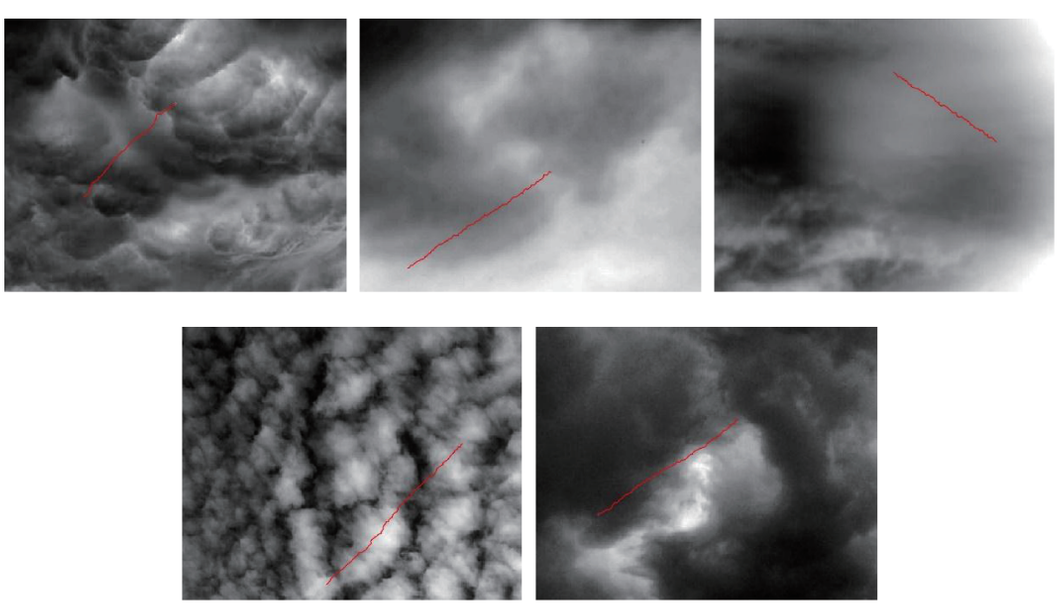

Fig.9 Track of five sequences
图9 五个序列图像轨迹

include a total of 410 images also confirmed our method to be 5-12 times more effective than other methods. Counting the probability of detection of the five sequences also indicated our method to be significantly more ac-

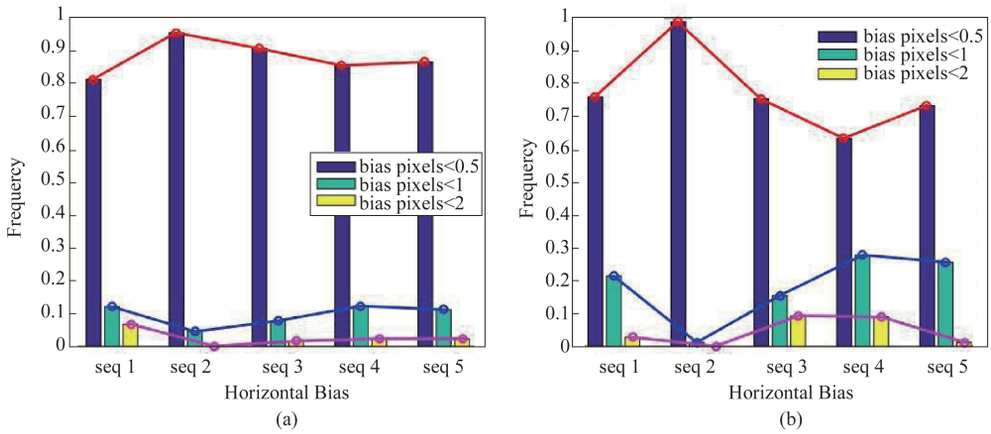

Fig. 10 Histograms of detected bias pixels obtained by using our method (a) histograms of horizontal detected bias pixels of five sequences, (b) histograms of vertical detected bias pixels of five sequences
图10 本文方法处理后像素偏差的柱状图(a)五个序列的水平方向偏差柱状图,(b)五个序列的垂直方向偏差柱状图

curate than other methods, with $\overline{\mathrm{SNR}_{\mathrm{in}}}$ = 1.44 and the average detection probability of our algorithms of 95.71%. The method proposed in this paper has a good effect on the image with obvious grayscale fluctuation in adjacent regions. For images with small fluctuations, the method of this paper needs further improvement. In future research, we plan to develop a more effective detection algorithm for multi-target complex background and occlusion based on the single-frame detection method proposed in this paper.

References

[1] Gao C Q, Meng D Y, Yang Y, *et al*. Infrared patch-image model for small target detection in a single image[J]. *IEEE Transactions on Image Processing*, 2013, **22**(12), 4996-5009.

[2] Luo K P. Space-based infrared sensor scheduling with high uncertainly: Issues and challenges [J]. *Syst. Eng.*, 2015, **18** (1): 102-113.

[3] Gao F, Li H, Li T, *et al*. Infrared small target detection in compressive domain[J]. *Electron. Lett.*, 2014, **50**(7): 510-512.

[4] Gao C Q, Zhang T Q, Li Q. Small infrared target detection using sparse ring representation[J]. *IEEE Aerospace and Electronic Systems Magazine*, 2012, **27**(3): 21-30.

[5] Yang X, Zhou Y P, Zhou D K, *et al*. A new infrared small and dim target detection algorithm based on multi-directional composite window[J]. *Infrared Phys. Technol.*, 2015, **71**:402-407.

[6] Shao X P, Fan H, Lu G X, *et al*. An improved infrared dim and small target detection algorithm based on the contrast mechanism of human visual system [J]. *Infrared Phys. Technol.*, 2012, **55** (5), 403-408.

[7] Wang P, Tian J W, Gao C Q. Infrared small target detection using directional high pass filters based on LS-SVM [J]. *Electron. Lett.*, 2009, **45** (3), 156 - 158.

[8] WU Tian-Ai, HUANG Shu-Cai, YUAN Zhi-Wei, *et al*. NSCT combined with SVD for infrared dim target complex background suppression[J]. *Infrared Technology*(吴天爱,黄树彩,苑智玮,等。联合 *NSCT* 和 *SVD* 方法的红外弱小目标复杂背景抑制,**红外技术**), 2016,**38**(9):758-764.

[9] WANG Huai-Ye, ZHANG Ke, LI Yan-Jun. Anisotropic gaussian filtering for infrared image[J]. *Journal Infrared Millimeter & Waves* (王怀野,张科,李言俊.各向异性滤波在红外图像处理中的应用. **红外与毫米波学报**), 2005, **24**(2):109-113.

[10] Li Y, Song Y, Zhao Y F, *et al*. An infrared target detection algorithm based on lateral inhibition and singular value decomposition [J]. *Infrared Physics & Technology*, 2017, **85**:238-245.

[11] Chen Z M, Tian M C, Bo Y M, *et al*. Improved infrared small target detection and tracking method based on new intelligence particle filter[J]. *Computational Intelligence*, 2018,**34**(3):917-938.

[12] Zhao F, Lu H Z, Zhang Z Y, *et al*. Complex background suppression based on fusion of morphological Open filter and nucleus similar pixels bilateral filter[J]. *Infrared Physics & Technology*, 2012, **55**(6): 454-461.

[13] Bae, Tae-Wuk. Spatial and temporal bilateral filter for infrared small target enhancement [J]. *Infrared Physics & Technology*, 2014, **63** (2):42-53.

[14] Tian H B, Department E E, Amp H V. Infrared small target detection based on bilateral filter and bhattacharyya distance[J]. *Nuclear Electronics & Detection Technology*, 2014, **34**(10):1159-1163.

[15] Deng H, Wei Y T, Tong M W. Background suppression of small target image based on fast local reverse entropy operator[J]. *IET Computer Vision*, 2013, **7**(5): 405-413.

[16] Deng H, Liu J G, Chen Z. Infrared small target detection based on modified local entropy and EMD[J]. *Chinese Optical Letters*, 2010, **8** (1): 24-28.

[17] Li C J, Wei Y, Shi Z L. A small target detection algorithm based on multi-scale energy cross [J]. *IEEE Int. Conf. Robotics Intell. Syst. Signal Process*, 2003, **2**, 1191 - 1196.

[18] Bai X Z, Bi Y G. Derivative entropy-based contrast measure for infrared small-target detection[J]. *IEEE Transactions on Geoscience & Remote Sensing*, 2018, PP(99):1-15.

[19] Shang K, Sun X, Tian J W, *et al*. Infrared small target detection via line-based reconstruction and entropy-induced suppression [J]. *Infrared Physics & Technology*, 2016, **76**:75-81.

[20] Chen Z, Luo S, Xie T, *et al*. A novel infrared small target detection method based on BEMD and local inverse entropy[J]. *Infrared Physics & Technology*, 2014, **66**(9):114-124.

[21] Mao Y, Zheng M, Jia W, *et al*. Analysis of small target detection algorithm based on image gray entropy[C]. *IEEE International Conference on Electronic Measurement & Instruments*, 2016.

[22] Peng G H, Chen H, Wu Q. Infrared small target detection under complex background[J]. *Advanced Materials Research*, 2011, **346**: 615-619.

[23] Qu X J, Chen H, Peng G H. Novel detection method for infrared small targets using weighted information entropy[J]. *Journal of Systems Engineering and Electronics*, 2012, **23**(6): 838-842.

[24] Philip C L, Li H, Wei Y T, *et al*. A local contrast method for small infrared target detection [J]. *IEEE Trans. on Geoscience & Remote Sensing*, 2013, **52**(1): 574-581.

[25] Deng H, Sun X P, Liu M L, *et al*. Entropy-based window selection for detecting dim and small infrared targets[J]. *Pattern Recognition*, 2017, **61**:66-77.

[26] Deng H, Sun X P, Liu M L, *et al*. Infrared small-target detection using multiscale gray difference weighted image entropy [J]. *IEEE Transactions on Aerospace & Electronic Systems*, 2016, **52** (1): 60-72.

[27] Wang G Y. Efficient method for multiscale small target detection from a natural scene [J]. *Opt. Eng.* 1996, **35**(3): 761-768.

[28] Huang X P, Wang Y. *Kalman filter principle and application: MATLAB simulation* [M]. Publishing House of Electronics Industry. 2015.